Electronic Supplementary Information for

A cyano cobalt "electron transfer bridge" boosting the two-electron reaction of a MnO_2 cathode with long lifespan in aqueous zinc batteries

Yaozhi Liu,[a,b] Lu Lin,[a] Tengsheng Zhang,[b] Zhiqing Xue,[a] Jie Liu,[d,e] Dongliang Chao*[b] and Xiaoqi Sun*[a,c]

[a] Department of Chemistry, Northeastern University, 3-11 Wenhua Road, Shenyang, 110819, China.

[b] Laboratory of Advanced Materials, Shanghai Key Laboratory of Molecular Catalysis and Innovative Materials, and School of Chemistry and Materials, Fudan University, Shanghai 200433, China.

[c] National Frontiers Science Center for Industrial Intelligence and Systems Optimization, Northeastern University, 3-11 Wenhua Road, Shenyang, 110819, China.

[d] School of Resources and Civil Engineering, Northeastern University, 3-11 Wenhua Road, Shenyang, 110819, China.

[e] National-local Joint Engineering Research Center of High-efficient Exploitation Technology for Refractory Iron Ore Resources, Shenyang, 110819, China.

* E-mail: chaod@fudan.edu.cn; sunxiaoqi@mail.neu.edu.cn

Supplementary figures and tables

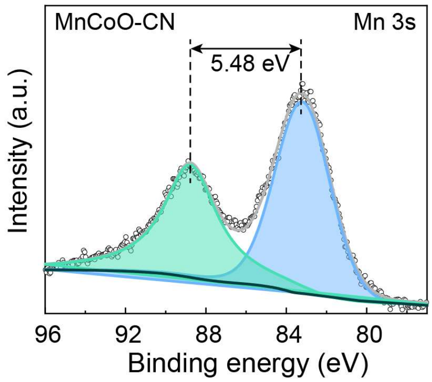

Figure S1. Mn 3s XPS of the MnCoO-CN material.

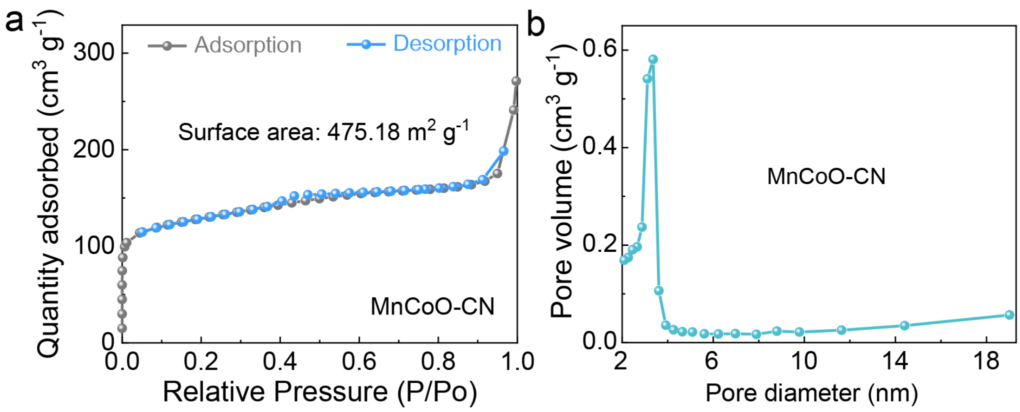

Figure S2. a) The N_2 adsorption-desorption isotherm and b) pore size distribution of the MnCoO-CN material.

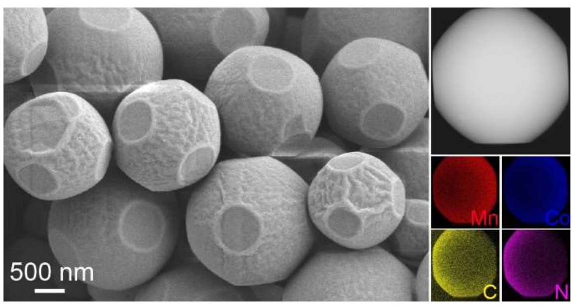

Figure S3. SEM image and STEM-EDS elemental mapping of the MnCo-PBA starting material.

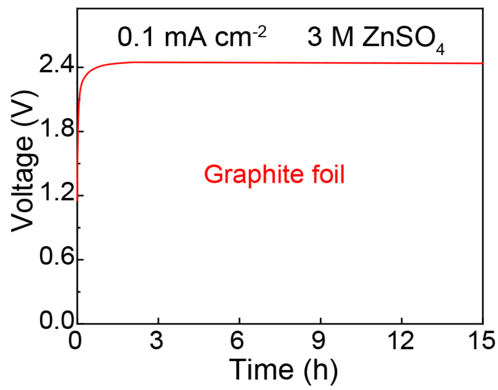

Figure S4. The oxidation process of the 3 M $ZnSO_4$ electrolyte with a graphite foil electrode.

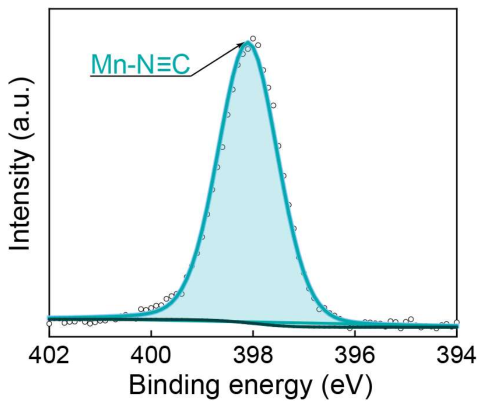

Figure S5. N 1s XPS of the MnCo-PBA starting material.

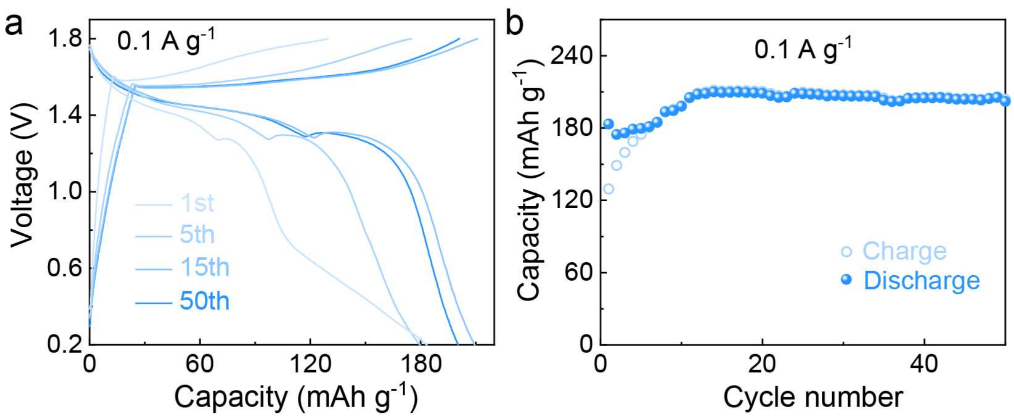

Figure S6. a) Charge-discharge curves and b) cycling performance of the MnCoO-CN cathode in 3 M $ZnSO_4$ at 0.1 A g^{-1} with the top voltage cut-off of 1.8 V.

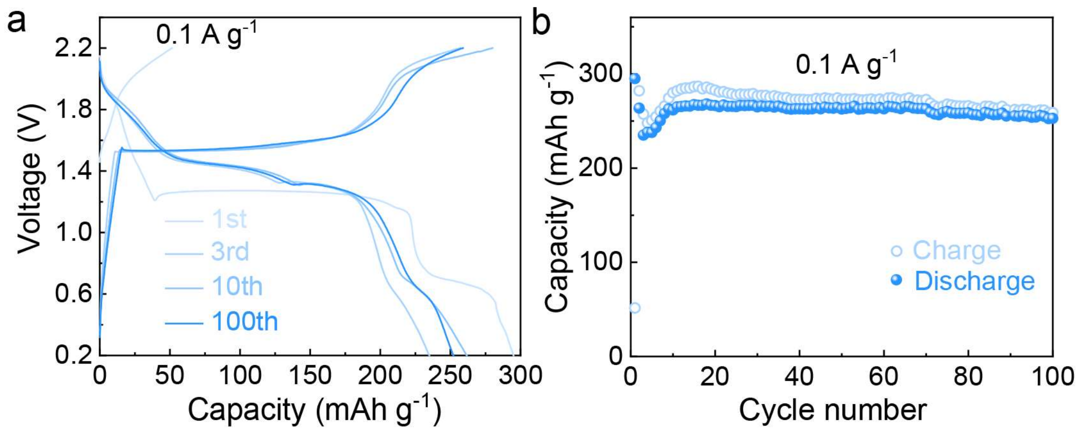

Figure S7. a) Charge-discharge curves and b) cycling performance of α-MnO_2 cathode in 3 M $ZnSO_4$ at 0.1 A g^{-1}.

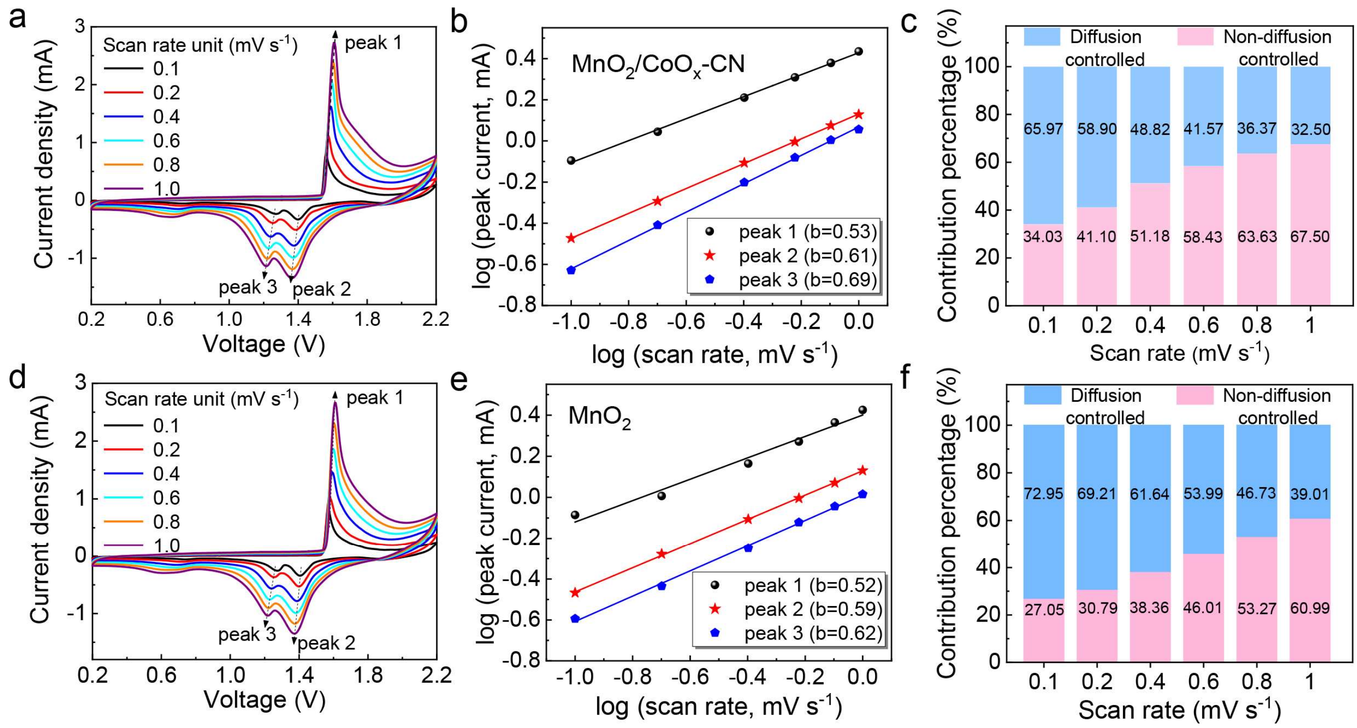

Figure S8. a,d) CV curves at different scan rates, b,e) the log(*i*) vs. log(*v*) plots of the three peaks and c,f) the non-diffusion and diffusion-controlled contributions at different scan rates of a-c) MnO_2/CoO_x-CN and d-f) MnO_2.

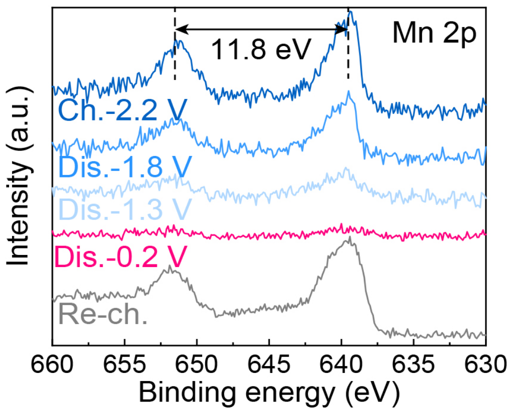

Figure S9. Mn 2p XPS of the MnO_2/CoO_x-CN cathode at different states.

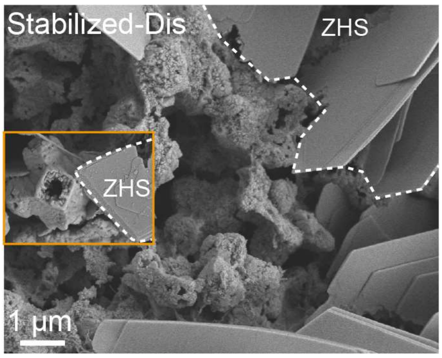

Figure S10. SEM image of the discharged MnO_2/CoO_x-CN cathode.

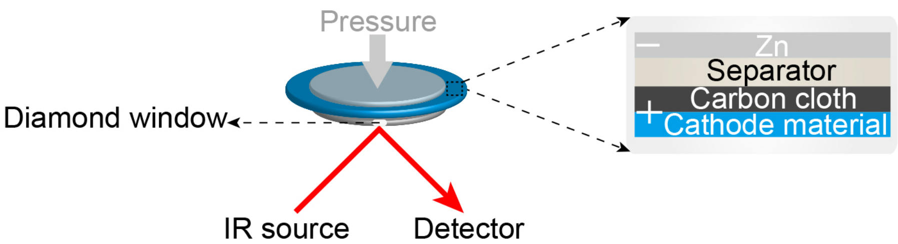

Figure S11. The in-situ ATR-FTIR setup.

Table S1 The weight percentages of Mn and Co in the MnCoO-CN composite by ICP-OES.

Element	wt%
Mn	50.9
Co	1.8

Estimation of capacity based on MnO_2 mass according to the results in Table S1:

According to ICP analysis, 50.9 wt% weight in the MnCoO-CN composite material is from Mn element. When all Mn transforms to MnO_2 after conditioning, the weight portion of MnO_2 with respect to the initial overall weight is 50.9 wt% ÷ M_{Mn} × M_{MnO_2} = 50.9 wt% ÷ 54.94 g mol^{-1} × 86.94 g mol^{-1} = 80.5%. The cathode delivers 425 mAh g^{-1} capacity after conditioning based on the initial composite mass, which corresponds to the capacity of 425 mAh g^{-1} ÷ 80.5% = 527 mAh g^{-1} based on the mass of MnO_2.

Table S2 Calculation of two-electron transfer contribution in MnO_2.

Cathode	MnO_2	MnO_2/CoO_x-CN
Mn concentration in electrolyte at the charged state (mM)	36.1	57.3
Mn concentration in electrolyte at the discharged state (mM)	95.7	183.6
Two-electron transfer mass (mg) = conc[diff] (mM) × 60 (μL) × 86.94 (g mol^{-1})	0.311	0.659
Overall MnO_2 mass (mg)	1.25	0.822
Two-electron transfer % = two-electron transfer mass ÷ overall MnO_2 mass × 100%	25%	80%

Discussion of Table S2:

To measure the Mn concentrations in the electrolyte at different states, the electrolyte in cycled cells is extracted from separators. The Mn/Zn ratios are measured by ICP, and the Zn concentration of 3 M is used as a reference to calculate Mn concentrations. The fluctuation of Zn concentration during charge/discharge is only a minority of the overall Zn content in the 3 M $ZnSO_4$ electrolyte. To be more specific, 60 μL electrolyte in the cell contains 60 μL × 3 M = 0.18 mmol of Zn. The MnO_2/CoO_x-CN cathode reaches the highest capacity around 0.433 mAh. This is the same as the Zn deposition capacity at the anode, which corresponds to 0.433 mAh ÷ 820 mAh g^{-1} ÷ 65.4 g mol^{-1} = 0.008 mmol of Zn. The concentration change in the electrolyte is only 0.008/0.18 = 5%, assuming no Zn participation in the cathode reaction. This change is small, and the utilization of Zn concentration as the reference to calculate Mn concentration is thus feasible.

During the two electron reaction of MnO_2, Mn^{2+} is formed during discharge, and its dissolution in the electrolyte causes Mn concentration increase. Upon charge, Mn^{2+} is oxidized and deposited back to the cathode as MnO_2, and Mn concentration in the electrolyte decreases. Therefore, the Mn concentration difference between the charged and discharged states is the active material undergoing reversible two-electron transfer of MnO_2/Mn^{2+} based on the dissolution/deposition reaction. The corresponding mass of MnO_2 is calculated based on the following equation:

$$m_{two\text{-}electron} = (c_{dis.} - c_{ch.}) \times V_{electrolyte} \times M_{MnO_2} \qquad \text{equation (1)}$$

The mass contribution of two-electron transfer in the total MnO_2 is calculated based on the following equation:

$$\omega_{two\text{-}electron} = \frac{m_{two\text{-}electron}}{m_{MnO_2}} \times 100\% \qquad \text{equation (2)}$$

In the above equations, $c_{dis.}$ and $c_{ch.}$ represent the Mn concentrations in electrolyte at the discharged and charged states, respectively; $V_{electrolyte}$ corresponds to the volume of electrolyte; M_{MnO_2} is the molecular weight of MnO_2; m_{MnO_2} is the MnO_2 mass.

Table S3 Capacity comparison of the MnO_2/CoO_x-CN cathode in the Mn^{2+} free electrolyte of 3 M $ZnSO_4$ with previously reported manganese oxide cathodes using electrolytes containing pre-added Mn^{2+} salts in aqueous zinc batteries.

Cathode material	Electrolyte	Current density/rate	Capacity	Ref.
Od-Mn_3O_4	2 M $ZnSO_4$ + 0.2 M $MnSO_4$	0.2 A g^{-1}	396 mAh g^{-1}	1
MO-ZMO	2 M $Zn(CF_3SO_3)_2$ + 0.1 M $MnSO_4$	0.1 A g^{-1}	247 mAh g^{-1}	2
$Mg_{0.9}Mn_3O_7 \cdot 2.7H_2O$	3 M $ZnSO_4$ + 0.1 M $MnSO_4$	0.2 A g^{-1}	312 mAh g^{-1}	3
BMO-6	2 M $ZnSO_4$ + 0.25 M $MnSO_4$	0.1 A g^{-1}	363 mAh g^{-1}	4
Cu-MnO_2	2 M $ZnSO_4$ + 0.3 M $MnSO_4$	0.1 A g^{-1}	443 mAh g^{-1}	5
PODA/MnO_2	2 M $ZnSO_4$ + 0.1 M $MnSO_4$	0.1 A g^{-1}	321 mAh g^{-1}	6
MnO_2/CoO_x-CN	3 M $ZnSO_4$	0.1 A g^{-1} 0.2 A g^{-1}	425 mAh g^{-1} 369 mAh g^{-1}	This work

Table S4 Cycling performance comparison of the MnO_2/CoO_x-CN cathode in the Mn^{2+} free electrolyte of 3 M $ZnSO_4$ with previously reported manganese oxide cathodes using electrolytes containing pre-added Mn^{2+} salts in aqueous zinc batteries.

Cathode material	Electrolyte	Current density/rate	Cycling performance	Ref.
Od-Mn_3O_4	2 M $ZnSO_4$ + 0.2 M $MnSO_4$	5.0 A g^{-1}	95.7% after 12000 cycles	1
$Mg_{0.9}Mn_3O_7 \cdot 2.7H_2O$	3 M $ZnSO_4$ + 0.1 M $MnSO_4$	0.2 A g^{-1} 5.0 A g^{-1}	95% after 100 cycles 92% after 5000 cycles	3
BMO-6	2 M $ZnSO_4$ + 0.25 M $MnSO_4$	1.0 A g^{-1}	93% after 10000 cycles	4
PANI-MnO_2	2 M $ZnSO_4$ + 0.1 M $MnSO_4$	0.2 A g^{-1} 2.0 A g^{-1}	89% after 200 cycles 83% after 5000 cycles	7
α-MnO_2	2 M $ZnSO_4$ + 0.1 M $MnSO_4$	5 C	92% after 5000 cycles	8
$Ca_{0.28}MnO_2$	1 M $ZnSO_4$ + 0.1 M $MnSO_4$	3.5 A g^{-1}	92% after 5000 cycles	9
CNT@KMO@GC	2 M $ZnSO_4$ + 0.2 M $MnSO_4$	10.0 A g^{-1}	80% after 10000 cycles	10
MnO_2	2 M $ZnSO_4$ + 0.005 M $MnSO_4$	10 mA cm^{-2}	100% after 16000 cycles	11
K-V_2C@MnO_2	2 M $ZnSO_4$ + 0.25 M $MnSO_4$	0.3 A g^{-1} 2.0 A g^{-1}	87% after 180 cycles 82% after 5000 cycles	12
MnO_2/CoO_x-CN	3 M $ZnSO_4$	0.2 A g^{-1} 2.0 A g^{-1}	81.6% after 300 cycles 83.1% after 25000 cycles	This work

References

1 Q. Tan, X. Li, B. Zhang, X. Chen, Y. Tian, H. Wan, L. Zhang, L. Miao, C. Wang, Y. Gan, J. Jiang, Y. Wang, H. Wang, *Adv. Energy Mater.* 2020, **10**, 2001050. **DOI:** 10.1002/aenm.202001050.

2 Y. Zeng, Y. Wang, Q. Jin, Z. Pei, D. Luan, X. Zhang, X. W. Lou, *Angew. Chem. Int. Ed.* 2021, **60**, 25793-25798. **DOI:** 10.1002/anie.202113487.

3 J. Li, N. Luo, L. Kang, F. Zhao, Y. Jiao, T. J. Macdonald, M. Wang, I. P. Parkin, P. R. Shearing, D. J. L. Brett, G. Chai, G. He, *Adv. Energy Mater.* 2022, **12**, 2201840. **DOI:** 10.1002/aenm.202201840.

4 Y. Ma, M. Xu, R. Liu, H. Xiao, Y. Liu, X. Wang, Y. Huang, G. Yuan, *Energy Stor. Mater.* 2022, **48**, 212-222. **DOI:** 10.1016/j.ensm.2022.03.024.

5 J. Zhang, W. Li, J. Wang, X. Pu, G. Zhang, S. Wang, N. Wang, X. Li, *Angew. Chem. Int. Ed.* 2023, **62**, e202215654. **DOI:** 10.1002/anie.202215654.

6 Y. Zhao, R. Zhou, Z. Song, X. Zhang, T. Zhang, A. Zhou, F. Wu, R. Chen, L. Li, *Angew. Chem. Int. Ed.* 2022, **61**, e202212231. **DOI:** 10.1002/anie.202212231.

7 J. Huang, Z. Wang, M. Hou, X. Dong, Y. Liu, Y. Wang, Y. Xia, *Nat. Commun*. 2018, **9**, 2906. **DOI:** 10.1038/s41467-018-04949-4.

8 H. Pan, Y. Shao, P. Yan, Y. Cheng, K. Han, Z. Nie, C. Wang, J. Yang, X. Li, P. Bhattacharya, K. T. Mueller, J. Liu, *Nat. Energy* 2016, **5**, 16039. **DOI:** 10.1038/NENERGY.2016.39.

9 T. Sun, Q. Nian, S. Zheng, J. Shi, Z. Tao, *Small* 2020, **16**, 200597. **DOI:** 10.1002/smll.202000597.

10 G. Wang, Y. Wang, B. Guan, J. Liu, Y. Zhang, X. Shi, C. Tang, G. Li, Y. Li, X. Wang, L. Li, *Small* 2021, **17**, 2104557. **DOI:** 10.1002/smll.202104557.

11 X. Shen, X. Wang, Y. Zhou, Y. Shi, L. Zhao, H. Jin, J. Di, Q. Li, *Adv. Funct. Mater.* 2021, **31**, 2101579. **DOI:** 10.1002/adfm.202101579.

12 X. Zhu, Z. Cao, W. Wang, H. Li, J. Dong, S. Gao, D. Xu, L. Li, J. Shen, M. Ye, *ACS Nano* 2021, **15**, 2971-2983. **DOI:** 10.1021/acsnano.0c09205.